

Article

Electrical Transport Measurements on Layered La(O,F)BiS₂ under Extremely High Pressure

Ryo Matsumoto ^{1,2,*}, Sayaka Yamamoto ^{2,3}, Yoshihiro Nemoto ⁴, Yuki Nishimiya ⁴ and Yoshihiko Takano ^{2,3}

¹ International Center for Young Scientists (ICYS), National Institute for Materials Science, Tsukuba 305-0047, Ibaraki, Japan

² International Center for Materials Nanoarchitectonics (MANA), National Institute for Materials Science, Tsukuba 305-0047, Ibaraki, Japan; sayaka12243@gmail.com (S.Y.); takano.yoshihiko@nims.go.jp (Y.T.)

³ Graduate School of Pure and Applied Sciences, University of Tsukuba, Tsukuba 305-8577, Ibaraki, Japan

⁴ Electron Microscopy Analysis Station, National Institute for Materials Science, Tsukuba 305-0047, Ibaraki, Japan; nemoto.yoshihiro@nims.go.jp (Y.N.); nishimiya.yuki@nims.go.jp (Y.N.)

* Correspondence: matsumoto.ryo@nims.go.jp

Abstract: Layered La(O,F)BiS₂ exhibits drastic enhancements of the superconducting transition temperature (T_c) under high pressure among the BiS₂-based superconducting family. However, the high-pressure application beyond a high- T_c phase of the monoclinic structure has not been conducted. In this study, the electrical transport properties in La(O,F)BiS₂ single crystal are measured under high pressures up to 83 GPa. An insulating phase without superconductivity is observed under a higher-pressure region above 16 GPa. Moreover, the sample exhibits metallicity and superconductivity above 60 GPa. The newly observed hidden semiconducting phase and reentrant superconductivity have attracted much attention in BiS₂-based compounds.

Keywords: superconductivity; high pressure; BiS₂



Citation: Matsumoto, R.; Yamamoto, S.; Nemoto, Y.; Nishimiya, Y.; Takano, Y. Electrical Transport Measurements on Layered La(O,F)BiS₂ under Extremely High Pressure. *Condens. Matter* **2022**, *7*, 25. <https://doi.org/10.3390/condmat7010025>

Academic Editor: Carmine Attanasio

Received: 24 January 2022

Accepted: 28 February 2022

Published: 2 March 2022

Publisher's Note: MDPI stays neutral with regard to jurisdictional claims in published maps and institutional affiliations.



Copyright: © 2022 by the authors. Licensee MDPI, Basel, Switzerland. This article is an open access article distributed under the terms and conditions of the Creative Commons Attribution (CC BY) license (<https://creativecommons.org/licenses/by/4.0/>).

1. Introduction

Layered BiS₂-based superconductors, represented as La(O,F)BiS₂ [1], have opened various materials science properties, such as their anomalous upper critical field [2,3], thermoelectric performance [4–6], topological features [7], and superconductivity on high-entropy alloys [8], up for further investigation. Among them, the performance of the material at high-pressures has attracted considerable attention. The superconducting transition temperature (T_c) in La(O,F)BiS₂ at ambient pressure is 2.5 K with maximum F-doping [1]. The original T_c is discretely enhanced with a structural phase transition from tetragonal to monoclinic [9]. Interestingly, the high-pressure phase and enhanced T_c are quenchable to ambient pressure via high-pressure synthesis or annealing at 600–700 °C and 2 GPa [10]. According to theoretical calculation [11] and experimental observation of the isotope effect [12], the pairing mechanism of superconductivity in the ambient tetragonal phase is unconventional. In contrast, the isotope effects on the high-pressure monoclinic phase suggest conventional phonon-mediated superconductivity [13]. Most layered BiS₂-based superconductors exhibit similar high-pressure effects [14–17]. Therefore, investigating the high-pressure effects on BiS₂-based materials is important for understanding its superconducting mechanism and increasing the maximum T_c .

The high-pressure study of La(O,F)BiS₂ is important because it has the highest T_c among the BiS₂-based superconductors. La(O,F)BiS₂ exhibits superconductivity with a maximum $T_c = 2.5$ K at ambient pressure by F doping into O in the parent compound of insulating LaOBiS₂ with a direct bandgap of 0.8–1.0 eV [1,18]. The electrical transport property under high pressure on polycrystalline La(O,F)BiS₂ has been investigated up to 18 GPa, and the T_c exhibits a “dome-like” feature [9]. T_c suddenly jumps up to 10.7 K by applying pressure at around 1 GPa, and monotonically decreased with increasing

the pressure up to 18 GPa. Recently, similar high-pressure effects of T_c enhancement and quench of higher- T_c phase have been reported for single-crystalline La(O,F)BiS₂ [19]. However, the high-pressure study of La(O,F)BiS₂ above 18 GPa beyond a high- T_c phase of the monoclinic structure has not been conducted.

A reemergence of superconductivity in a higher pressure region after the “dome-like” feature of T_c has been reported in several materials. It attracts considerable attention because different superconducting properties compared with the original T_c , for instance, higher T_c and robust superconductivity, are often observed. K_xFe₂Se₂ and (Li_{1-x}Fe_x)OHFe_{1-y}Se at ambient pressure exhibit superconductivity at 30 K and 41 K. The superconductivity in these materials is rapidly suppressed by applying pressure. After further compression, K_xFe₂Se₂ and (Li_{1-x}Fe_x)OHFe_{1-y}Se show reentrant superconductivity with higher T_c of 48.7 K and 50 K than those of the original superconducting phase [20–22]. Recently, highly robust reentrant superconductivity in quasi-2D kagome metal CsV₃Sb₅ has been reported [23]. Inspired by the discoveries of the reentrant superconductivity, we conducted electrical transport measurements on superconducting La(O,F)BiS₂ under high pressure of up to 83 GPa using a diamond anvil cell (DAC) with a boron-doped diamond micro-electrode. A reemergence of superconductivity was observed in La(O,F)BiS₂ under 60 GPa. The in-situ Raman spectroscopy under high pressure and transmission electron microscope (TEM) observation of the recovered sample were performed to analyze the crystal structure.

2. Experimental Procedures

La(O,F)BiS₂ single crystals were grown using the high-temperature flux method based on that reported in the literature [24,25]. The starting materials of La₂S₃, Bi, Bi₂S₃, Bi₂O₃, and BiF₃ were weighed with a nominal composition of LaO_{0.5}F_{0.5}BiS₂ (total 0.8 g). CsCl and KCl flux with a molar ratio of 5:3 (total 5 g) were mixed using a mortar and were sealed in a quartz tube. The sample was heated at 900 °C for 10 h, cooled slowly to 600 °C at a rate of 1 °C/h, and then naturally cooled to room temperature in the furnace. The products were washed using distilled water after the sample was opened in the air. For comparison, the undoped LaOBiS₂ was also synthesized using the same method.

The chemical compositions of the products were determined by scanning electron microscopy (SEM) equipped with energy-dispersive X-ray spectroscopy (EDX) using a JSM-6010LA (JEOL) instrument. An X-ray diffraction (XRD) pattern of the obtained sample was collected using a Mini Flex 600 (Rigaku) with Cu K α radiation ($\lambda = 1.5418 \text{ \AA}$). Refinement of the lattice parameters was performed by a Rietveld analysis using RIETAN-FP program [26]. In refinement, the tiny impurity peaks near 27° were excluded. The temperature dependence of the resistance in the range of 300 to 0.2 K at ambient pressure was measured by a four-probe method using an adiabatic demagnetization refrigerator option on a physical properties measurement system (Quantum Design). The high-pressure generation and the in-situ transport measurements were performed using a DAC with boron-doped diamond electrodes [27–29]. The anvil culet and gasket hole had diameters of 300 μm and 200 μm , respectively. The sample space was composed of SUS316 stainless steel, a cubic boron nitride pressure-transmitting medium, and a ruby powder pressure sensor. The generated pressure was determined using the ruby fluorescence method [30] and Raman shift of diamond [31] at room temperature. The Raman spectrum of the sample and fluorescence spectrum of ruby were acquired using an inVia Raman microscope (RENISHAW). TEM observation and atomic-resolution EDX mapping were conducted for the recovered sample from DAC using JEM-ARM200F (JEOL) to analyze the sample crystal structure further. The sample fabrication for TEM observation was performed using focused ion beam (FIB) apparatus JIB-4000 (JEOL).

3. Results and Discussion

The obtained sample of $\text{La}(\text{O},\text{F})\text{BiS}_2$ was evaluated at ambient pressure using the SEM/EDX observation, XRD analysis, and transport measurements. The inset of Figure 1a shows an SEM image of the obtained $\text{La}(\text{O},\text{F})\text{BiS}_2$ single crystal exhibiting a well-developed plate-like shape. The compositional ratio (La:Bi:S) was determined as 1:0.99:1.72 by normalizing La = 1 in the EDX analysis, which is consistent with the nominal cation composition. The upper pattern of Figure 1a shows the XRD signal from one piece of $\text{La}(\text{O},\text{F})\text{BiS}_2$ single crystal. The pattern only exhibited $00l$ diffraction peaks, indicating that the sample was a highly oriented crystal. The middle data of Figure 1a show the XRD pattern of the powdered $\text{La}(\text{O},\text{F})\text{BiS}_2$ single crystal with the fitting result of the Rietveld refinement. The green bars and blue spectrum indicate a peak position of the determined structure and a differential curve for the fitting. The analysis revealed that the sample crystallized with a tetragonal structure. The obtained lattice parameters and reliability factor were $a = 4.0729(2)$ Å, $c = 13.5001(16)$ Å, $R_{\text{wp}} = 10.3\%$. The EDX and XRD analyses establish that single crystal $\text{La}(\text{O},\text{F})\text{BiS}_2$ was obtained.

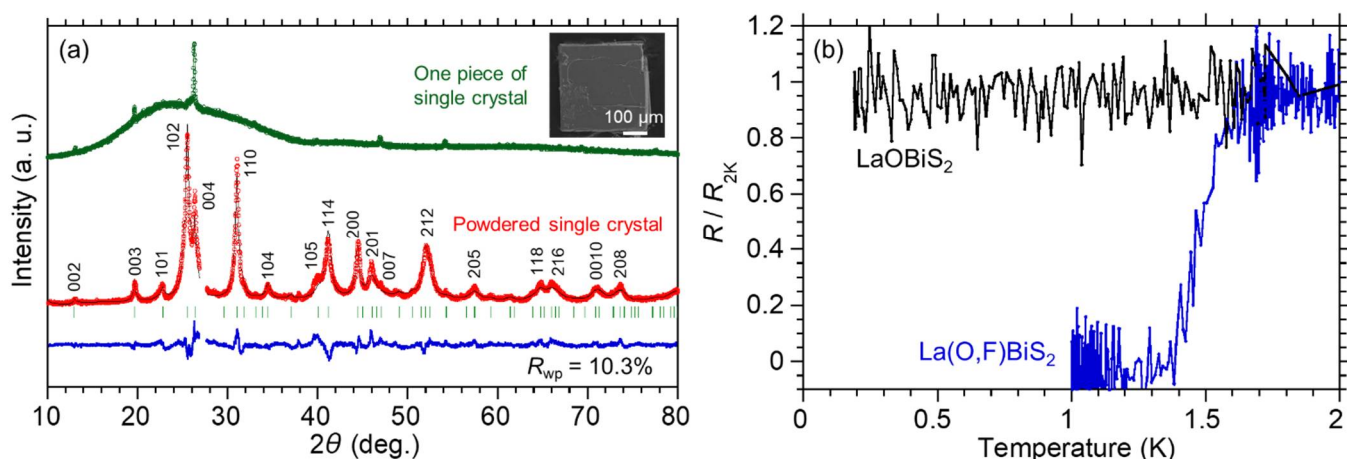


Figure 1. (a) XRD patterns with Cu $K\alpha$ radiation ($\lambda = 1.5418$ Å) of the obtained $\text{La}(\text{O},\text{F})\text{BiS}_2$. The upper pattern is from one piece of single crystal. The middle data show the pattern from the powdered single crystal with the fitting result of Rietveld refinement. The green bars and blue spectrum indicate a peak position of the determined structure and a differential curve for the fitting. The inset shows an SEM image for one piece of single crystal. (b) Temperature dependence of normalized resistance in $\text{La}(\text{O},\text{F})\text{BiS}_2$ and LaOBiS_2 single crystals at ambient pressure.

Figure 1b shows the temperature dependence of normalized resistance at ambient pressure in single crystal of $\text{La}(\text{O},\text{F})\text{BiS}_2$, and undoped LaOBiS_2 as a reference. The undoped LaOBiS_2 exhibited no superconductivity down to 0.2 K. In contrast, the doped sample $\text{La}(\text{O},\text{F})\text{BiS}_2$, at ambient pressure, exhibited an onset T_c of 1.7 K. According to the detailed structural analysis using a single crystalline XRD in the literature [25], $\text{LaO}_{1-x}\text{F}_x\text{BiS}_2$ with an actual F concentration $x \sim 0.23$ and ~ 0.46 show the lattice constant $c = 13.547(4)$ and $13.345(4)$ Å, respectively. The actual F concentration x of the obtained crystal in this study was estimated to be less than 0.23 because the lattice constant $c = 13.5001(16)$ Å was smaller than that of the previous report. In addition, based on the relationship between T_c and the amount of F (x) in the $\text{LaO}_{1-x}\text{F}_x\text{BiS}_2$ single crystal reported in the literature [32], the value of x was estimated to be less than 0.23, which was consistent with the estimated value from the XRD analysis.

Figure 2a shows the temperature dependence of resistance in $\text{La}(\text{O},\text{F})\text{BiS}_2$ single crystal under high pressure of 7.0 to 37 GPa. The sample exhibits a sharp drop to zero resistance at 7.0 GPa, corresponding to superconductivity. T_c is drastically enhanced from that of ambient pressure because of the structural phase transition, as reported in a previous high-pressure study on single crystals [19]. T_c monotonically decreased with the increasing

pressure of up to 13 GPa, consistent with the report on polycrystalline samples [9]. The superconducting transition could not be observed in the measured temperature range above 16 GPa, and the temperature dependence of the resistance exhibited a semiconducting tendency. In contrast, the semiconducting behavior was suppressed under further compression above 37 GPa, as seen in Figure 2b. At 60 GPa, a reemergence of superconducting transition was observed at around 3 K. In general, the pressure distribution in the sample chamber was quite large and affected the measured resistance under the extremely high-pressure region of the DAC. In particular, the semiconducting feature often remained after the insulator to metal transition due to the pressure distribution [33]. Therefore, the sample was considered to be metallic above 60 GPa, although the temperature dependence of the resistance was still semiconducting. As T_c gradually increased, the resistance at the lowest temperature approached zero with the increasing pressure up to 83 GPa. The appeared drop of resistance was gradually suppressed by applying a magnetic field, as represented in Figure 2c. Such suppression was further evidence of the higher-pressure phase of superconductivity in La(O,F)BiS₂. The inset of Figure 2c shows the temperature dependence of the upper critical field B_{c2} . T_{cS} was determined from the intersection point between the straight line of the normal resistance region and the extended line from resistance after the superconducting transition. $B_{c2}(0)$ was estimated to be 2.6 T under 79 GPa from the parabolic fitting. From the Ginzburg–Landau (GL) formula, $B_{c2}(0) = \Phi_0/2\pi\xi(0)^2$, where Φ_0 is the fluxoid and the coherence length at zero temperature $\xi(0)$ is estimated to be 11.2 nm.

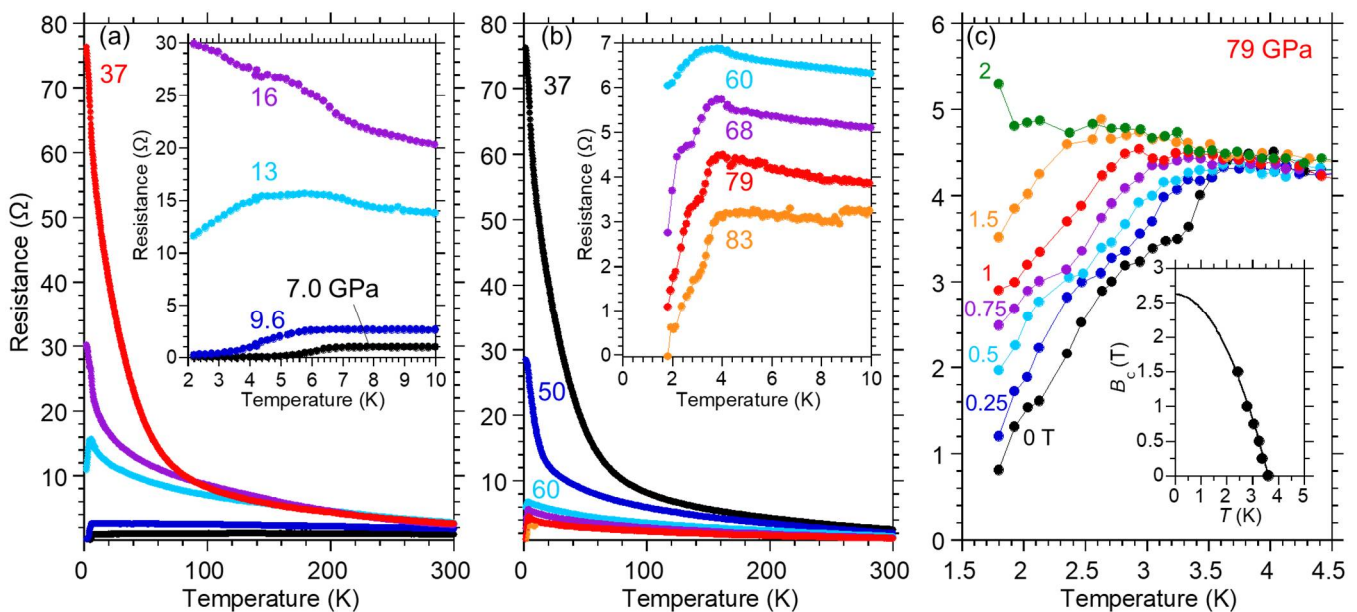


Figure 2. Temperature dependence of resistance in La(O,F)BiS₂ single crystal under high pressure between (a) 7.0 to 37 GPa, (b) 37 to 83 GPa, and (c) 79 GPa under various magnetic fields up to 2 T. The insets of (a,b) show the magnified plots around the low superconducting transition. The inset of (c) is the temperature dependence of the upper critical field B_{c2} .

Raman spectroscopy is often used to discuss the structure and vibration modes in the BiS₂-based compounds [19,34,35]. Figure 3a displays the Raman spectra of the La(O,F)BiS₂ single crystal up to 83 GPa from the ambient pressure. At ambient pressure, La(O,F)BiS₂ exhibited a Raman-active mode of A_{1g} originating from the in-plane vibrations of Bi and S atoms at the gamma point [34]. At ambient pressure, the peaks at around 70 cm⁻¹ and 123 cm⁻¹ were clearly visible, identified as A_{1g} symmetry. The positions of the corresponding peaks were slightly shifted to a higher wavenumber at 1.2 GPa. As reported in precise Raman analysis for La(O,F)BiS₂ single crystal [19], the original A_{1g} mode disappeared, and new peaks appeared at 2.7 GPa. The change in the Raman spectrum suggested the struc-

tural phase transition from tetragonal to monoclinic with the discrete enhancement of T_c in $\text{La}(\text{O},\text{F})\text{BiS}_2$. The observed peaks gradually shifted to a higher wavenumber with increasing the pressure up to 9.6 GPa. The intensity of the Raman peaks from the monoclinic structure became small above 13 GPa, suggesting an emergence of a new structure corresponding to the semiconducting phase without superconductivity. All the Raman peaks disappeared under further compression above 60 GPa, signaling another new structure or metallization. The reemergence of superconducting transition was observed in this pressure range. When pressure decreased to 15 GPa and ambient pressure, the Raman peaks were not recovered.

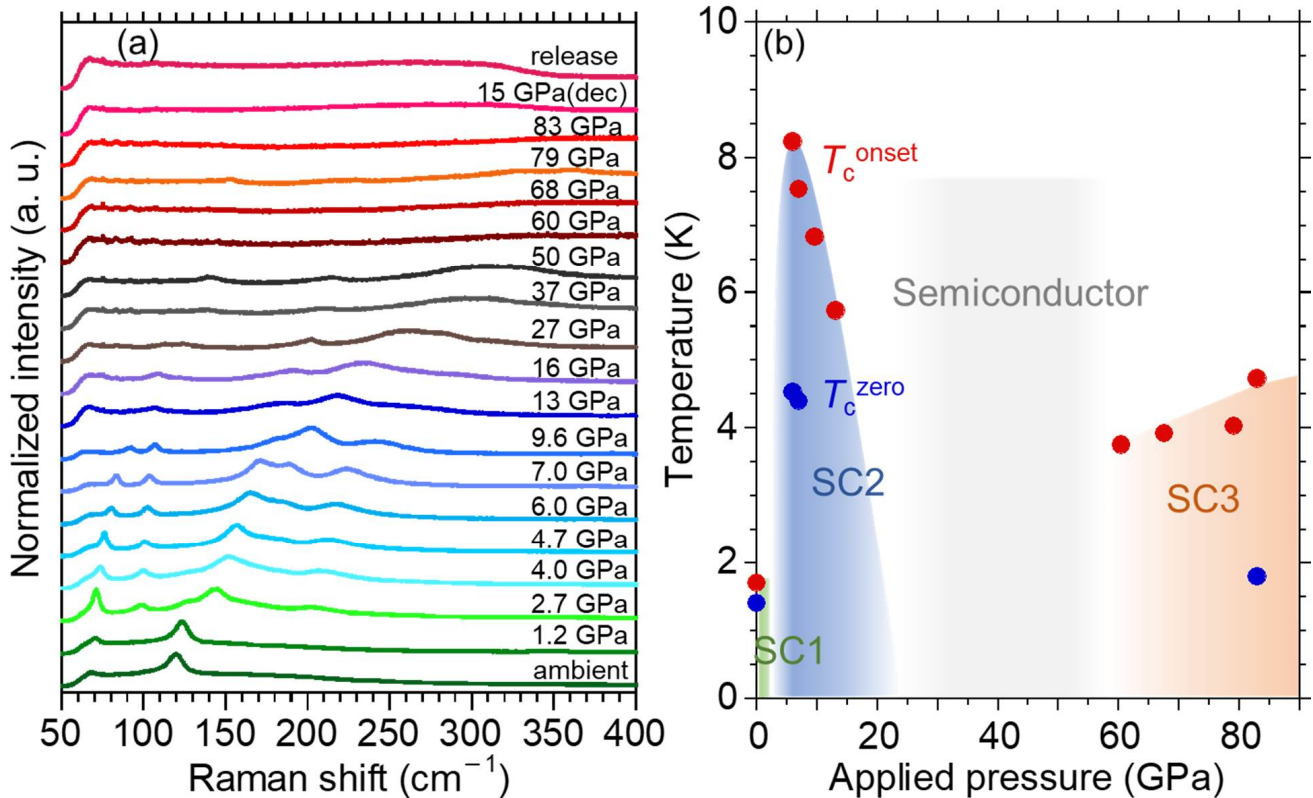


Figure 3. (a) Raman spectra of $\text{La}(\text{O},\text{F})\text{BiS}_2$ single crystal up to 83 GPa from the ambient pressure. The peak labeled “15 GPa(dec)” are the data from the decompression process. (b) Pressure dependence of T_c^{onset} and T_c^{zero} in $\text{La}(\text{O},\text{F})\text{BiS}_2$ single crystal up to 83 GPa.

Figure 3b shows the pressure dependence of T_c in $\text{La}(\text{O},\text{F})\text{BiS}_2$ single crystal up to 83 GPa. At ambient pressure, the original T_c with a tetragonal structure is 1.7 K (SC1). The T_c is suddenly enhanced up to 8.2 K with applied pressure above 1 GPa due to the phase transition to a monoclinic structure (SC2). The steep reduction of T_c with increasing the pressure in the monoclinic phase up to 13 GPa was possibly due to a phonon-hardening effect in conventional Bardeen–Cooper–Schrieffer type superconductors [36,37], as seen in the Raman analysis. The sample exhibited a semiconducting nature without superconductivity between 16 GPa and 50 GPa. Above 60 GPa, reentrant superconductivity was observed (SC3). Although the T_c s of SC3 was not higher than that of SC2, as in the case of Fe-based materials [20–22], quite robust pressure dependence of T_c against the pressure was confirmed, such as Kagome metal [23]. In addition, the reentrant T_c continued to enhance with increasing the pressure up to 83 GPa. For future research, the further application of pressure is expected to present the “dome-like” feature of T_c in the SC3 phase of $\text{La}(\text{O},\text{F})\text{BiS}_2$.

The TEM observation was conducted for the recovered sample of $\text{La}(\text{O},\text{F})\text{BiS}_2$ and as-grown $\text{La}(\text{O},\text{F})\text{BiS}_2$ single crystal in order to understand the origin of phase “SC3”. Figure 4a,b displays the scanning ion microscope images (SIM) of the as-grown and recovered $\text{La}(\text{O},\text{F})\text{BiS}_2$ single crystals before the TEM observation, respectively. The specimens were fabricated from the square region in (a) and (b) by the FIB, and their cross-sections were analyzed as seen in (c) and (d), respectively. Figure 4e shows a high-angle annular dark-field scanning TEM image taken with the incident beam parallel to the $[10]$ direction of the as-grown $\text{La}(\text{O},\text{F})\text{BiS}_2$ single crystal. No distortion and stacking faults were observed in the scanning TEM image for the analyzed area. In contrast, the scanning TEM image for the recovered sample was highly distorted with amorphous parts, as seen in Figure 4f. Such an amorphous-like structure can be seen in the broader region in the recovered sample (see Figure S1). This is consistent with the disappearance of Raman peaks above 60 GPa. Figure 4g,h shows the atomic-resolution EDX mapping for certain expanded parts of the as-grown and recovered samples. The layered structure composed of alternate stacks of conducting layers BiS_2 and reservoir blocking layers $\text{La}(\text{O},\text{F})$ was observed in both samples. Here, the blocking layer ($\text{La},\text{O},\text{F}$) in the recovered sample seemed to become thin compared with the original one (images with guidelines for the comparison are seen in Figure S2). The in-situ observation of the crystal structure under the pressure corresponding to phase “SC3” using XRD was expected in the future for a more detailed discussion on the origin of the reentrant superconductivity.

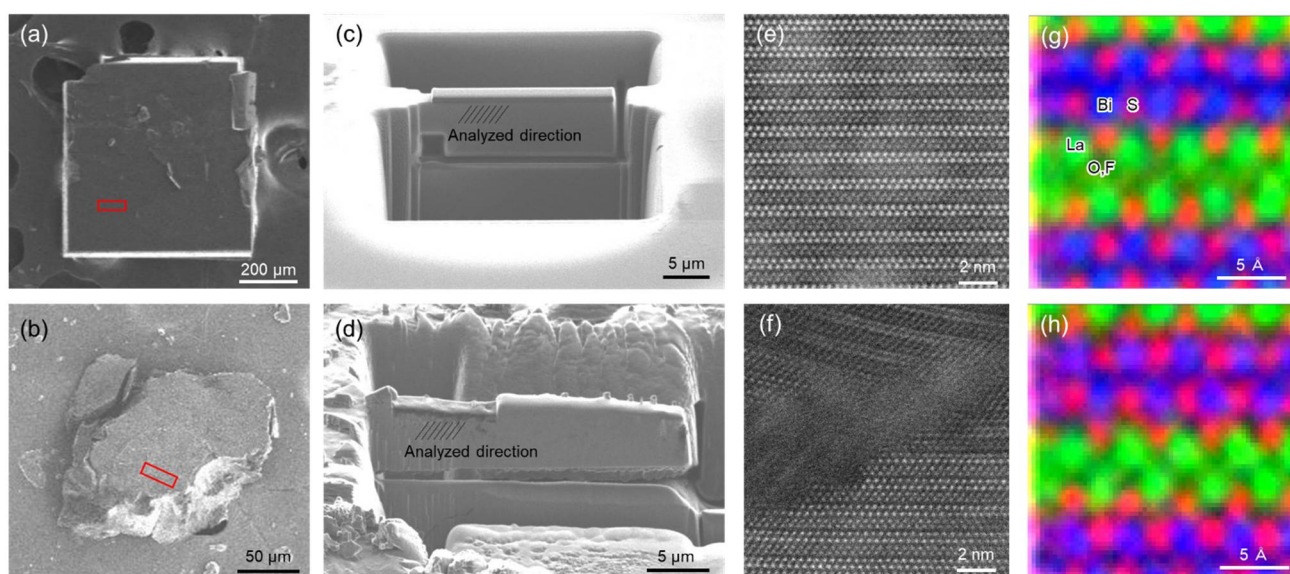


Figure 4. Scanning ion microscope images (SIM) of the (a) as-grown and (b) recovered $\text{La}(\text{O},\text{F})\text{BiS}_2$ single crystals. SIM images of the specimen for TEM observation of the (c) as-grown and (d) recovered samples. High-angle annular dark-field scanning TEM images for the (e) as-grown and (f) recovered samples. Atomic-resolution EDX mapping images for the (g) as-grown and (h) recovered samples.

4. Conclusions

The electrical transport property in layered $\text{La}(\text{O},\text{F})\text{BiS}_2$ single crystal was investigated under high pressure up to 83 GPa. The existence of a high-pressure phase with a higher T_c of this material has already been investigated. This study successfully observed the high-pressure semiconducting phase without superconductivity and the reentrant superconductivity. The semiconducting phase exhibited different Raman peaks from the superconducting monoclinic structure. In addition, the reentrant superconducting phase showed no Raman peak, and the recovered sample had an amorphous-like morphology. Therefore, the crystal structures of newly observed phases were different from the original tetragonal and monoclinic structures. Because the reentrant superconductivity was robust against the pressure and the T_c continued to enhance up to 83 GPa, further appli-

cation of pressure was expected. As a future investigation, the in-situ XRD analysis is expected to explain the origin of the reentrant superconductivity. The discovery of two high-pressure phases is important in order to understand further physics in the BiS₂-based superconductors.

Supplementary Materials: The following supporting information can be downloaded at: <https://www.mdpi.com/article/10.3390/condmat7010025/s1>, Figure S1: Wide view of high-angle annular dark field scanning TEM images for the recovered samples, Figure S2: Comparison between two EDX mapping images with a guideline of the blocking layers.

Author Contributions: Conceptualization, R.M.; Data curation, S.Y.; Investigation, R.M., S.Y., Y.N. (Yoshihiro Nemoto) and Y.N. (Yuki Nishimiya); Resources, Y.T.; Supervision, Y.T.; Visualization, R.M. and S.Y.; Writing—original draft, R.M.; Writing—review & editing, S.Y. All authors have read and agreed to the published version of the manuscript.

Funding: This research was funded by Japan Science and Technology Agency grant number JPMJMI17A2 and Japan Society for the Promotion of Science grant number 19H02177, 20H05644, and 20K22420.

Data Availability Statement: The data that support the findings of this study are available from the corresponding author upon reasonable request.

Acknowledgments: This work was partly supported by the JST-Mirai Program (grant no. JPMJMI17A2) and JSPS KAKENHI (grant nos. 19H02177, 20H05644, and 20K22420). The fabrication of the diamond electrodes was partly supported by the NIMS Nanofabrication Platform in Nanotechnology Platform Project sponsored by the Ministry of Education, Culture, Sports, Science, and Technology (MEXT), Japan. The TEM observation was carried out with the support of NIMS Electron Microscopy Analysis Station, Nanostructural Characterization Group. R.M. would like to acknowledge ICYS Research Fellowship, NIMS, Japan.

Conflicts of Interest: The authors declare no conflict of interest.

References

1. Mizuguchi, Y.; Demura, S.; Deguchi, K.; Takano, Y.; Fujihisa, H.; Gotoh, Y.; Izawa, H.; Miura, O. Superconductivity in Novel BiS₂-Based Layered Superconductor LaO_{1-x}F_xBiS₂. *J. Phys. Soc. Jpn.* **2012**, *81*, 114725. [[CrossRef](#)]
2. Mizuguchi, Y.; Miyake, A.; Akiba, K.; Tokunaga, M.; Kajitani, J.; Miura, O. Anisotropic upper critical field of the BiS₂-based superconductor LaO_{0.5}F_{0.5}BiS₂. *Phys. Rev. B* **2014**, *89*, 174515. [[CrossRef](#)]
3. Matsumoto, R.; Yamamoto, S.; Adachi, S.; Sakai, T.; Irifune, T.; Takano, Y. Diamond anvil cell with boron-doped diamond heater for high-pressure synthesis and in situ transport measurements. *Appl. Phys. Lett.* **2021**, *119*, 053502. [[CrossRef](#)]
4. Nishida, A.; Miura, O.; Lee, C.-H.; Mizuguchi, Y. High thermoelectric performance and low thermal conductivity of densified LaOBiS₂. *Appl. Phys. Express* **2015**, *8*, 111801. [[CrossRef](#)]
5. Goto, Y.; Miura, A.; Sakagami, R.; Kamihara, Y.; Moriyoshi, C.; Kuroiwa, Y.; Mizuguchi, Y. Synthesis, Crystal Structure, and Thermoelectric Properties of Layered Antimony Selenides REOSbSe₂ (RE = La, Ce). *J. Phys. Soc. Jpn.* **2018**, *87*, 074703. [[CrossRef](#)]
6. Matsumoto, R.; Nagao, M.; Ochi, M.; Tanaka, H.; Hara, H.; Adachi, S.; Nakamura, K.; Murakami, R.; Yamamoto, S.; Irifune, T.; et al. Pressure-induced insulator to metal transition of mixed valence compound Ce(O,F)SbS₂. *J. Appl. Phys.* **2019**, *125*, 075102. [[CrossRef](#)]
7. Yang, Y.; Wang, W.-S.; Xiang, Y.-Y.; Li, Z.-Z.; Wang, Q.-H. Triplet pairing and possible weak topological superconductivity in BiS₂-based superconductors. *Phys. Rev. B* **2013**, *88*, 094519. [[CrossRef](#)]
8. Sogabe, R.; Goto, Y.; Mizuguchi, Y. Superconductivity in REO_{0.5}F_{0.5}BiS₂ with high-entropy-alloy-type blocking layers. *Appl. Phys. Express* **2018**, *11*, 053102. [[CrossRef](#)]
9. Tomita, T.; Ebata, M.; Soeda, H.; Takahashi, H.; Fujihisa, H.; Gotoh, Y.; Mizuguchi, Y.; Izawa, H.; Miura, O.; Demura, S.; et al. Pressure-Induced Enhancement of Superconductivity and Structural Transition in BiS₂-Layered LaO_{1-x}F_xBiS₂. *J. Phys. Soc. Jpn.* **2014**, *83*, 063704. [[CrossRef](#)]
10. Mizuguchi, Y.; Hiroi, T.; Kajitani, J.; Takatsu, H.; Kadowaki, H.; Miura, O. Stabilization of high-T_c phase of BiS₂-based superconductor LaO_{0.5}F_{0.5}BiS₂ using high-pressure synthesis. *J. Phys. Soc. Jpn.* **2014**, *83*, 053704. [[CrossRef](#)]
11. Morice, C.; Akashi, R.; Koretsune, T.; Saxena, S.S.; Arita, R. Weak phonon-mediated pairing in BiS₂ superconductor from first principles. *Phys. Rev. B* **2017**, *95*, 180505. [[CrossRef](#)]
12. Hoshi, K.; Goto, Y.; Mizuguchi, Y. Selenium isotope effect in the layered bismuth chalcogenide superconductor LaO_{0.6}F_{0.4}Bi(S,Se)₂. *Phys. Rev. B* **2018**, *97*, 094509. [[CrossRef](#)]

13. Yamashita, A.; Usui, H.; Hoshi, K.; Goto, Y.; Kuroki, K.; Mizuguchi, Y. Possible pairing mechanism switching driven by structural symmetry breaking in BiS₂-based layered superconductors. *Sci. Rep.* **2021**, *11*, 230. [[CrossRef](#)] [[PubMed](#)]
14. Demura, S.; Deguchi, K.; Mizuguchi, Y.; Sato, K.; Honjyo, R.; Yamashita, A.; Yamaki, T.; Hara, H.; Watanabe, T.; Denholme, S.J.; et al. Coexistence of Bulk Superconductivity and Magnetism in CeO_{1-x}F_xBiS₂. *J. Phys. Soc. Jpn.* **2015**, *84*, 024709. [[CrossRef](#)]
15. Tanaka, M.; Nagao, M.; Matsumoto, R.; Kataoka, N.; Ueta, I.; Tanaka, H.; Watauchi, S.; Tanaka, I.; Takano, Y. Superconductivity and its enhancement under high pressure in “F-free” single crystals of CeOBiS₂. *J. Alloy. Compd.* **2017**, *722*, 467–473. [[CrossRef](#)]
16. Fujioka, M.; Matsumoto, R.; Yamaki, T.; Denholme, S.J.; Tanaka, M.; Takeya, H.; Yamaguchi, T.; Takahashi, H.; Takano, Y. Observation of a Pressure-Induced Phase Transition for Single Crystalline LaO_{0.5}F_{0.5}BiSeS Using a Diamond Anvil Cell. *J. Phys. Soc. Jpn.* **2015**, *84*, 95001. [[CrossRef](#)]
17. Selvan, G.K.; Kanagaraj, M.; Muthu, S.E.; Jha, R.; Awana, V.P.S.; Arumugam, S. Hydrostatic pressure effect on T_c of new BiS₂-based Bi₄O₄S₃ and NdO_{0.5}F_{0.5}BiS₂ layered superconductors. *Phys. Status Solidi* **2013**, *RRL* 7, 510.
18. Miura, A.; Mizuguchi, Y.; Takei, T.; Kumada, N.; Magome, E.; Moriyoshi, C.; Kuroiwa, Y.; Tadanaga, K. Structures and optical absorption of Bi₂OS₂ and LaOBiS₂. *Solid State Commun.* **2016**, *227*, 19–22. [[CrossRef](#)]
19. Yamamoto, S.; Matsumoto, R.; Adachi, S.; Takano, Y. High-pressure effects on La(O,F)BiS₂ single crystal using diamond anvil cell with dual-probe diamond electrodes. *Appl. Phys. Express* **2021**, *14*, 043001. [[CrossRef](#)]
20. Sun, L.; Chen, X.-J.; Guo, J.; Gao, P.; Huang, Q.-Z.; Wang, H.; Fang, M.; Chen, X.; Chen, G.; Wu, Q.; et al. Re-emerging superconductivity at 48 kelvin in iron chalcogenides. *Nature* **2012**, *483*, 67–69. [[CrossRef](#)]
21. Sun, J.; Shahi, P.; Zhou, H.; Huang, Y.; Chen, K.; Wang, B.; Ni, S.; Li, N.; Zhang, K.; Yang, W.; et al. Reemergence of high-T_c superconductivity in the (Li_{1-x}Fe_x)OHFe_{1-y}Se under high pressure. *Nat. Commun.* **2018**, *9*, 380. [[CrossRef](#)] [[PubMed](#)]
22. Shahi, P.; Sun, J.; Wang, S.; Jiao, Y.; Chen, K.; Sun, S.; Lei, H.; Uwatoko, Y.; Wang, B.; Cheng, J. High-T_c superconductivity up to 55 K under high pressure in a heavily electron doped Li_{0.36}(NH₃)_yFe₂Se₂ single crystal. *Phys. Rev. B* **2018**, *97*, 020508(R). [[CrossRef](#)]
23. Chen, X.; Zhan, X.; Wang, X.; Deng, J.; Liu, X.-B.; Chen, X.; Guo, J.-G.; Chen, X. Highly Robust Reentrant Superconductivity in CsV₃Sb₅ under Pressure. *Chin. Phys. Lett.* **2021**, *38*, 057402. [[CrossRef](#)]
24. Nagao, M.; Miura, A.; Demura, S.; Deguchi, K.; Watauchi, S.; Takei, T.; Takano, Y.; Kumada, N.; Tanaka, I. Growth and superconducting properties of F-substituted ROBiS₂ (R=La, Ce, Nd) single crystals. *Solid State Commun.* **2013**, *178*, 33–36. [[CrossRef](#)]
25. Miura, A.; Nagao, M.; Takei, T.; Watauchi, S.; Tanaka, I.; Kumada, N. Crystal structures of LaO_{1-x}F_xBiS₂ (x~0.23, 0.46): Effect of F doping on distortion of Bi-S plane. *J. Solid State Chem.* **2014**, *212*, 213–217. [[CrossRef](#)]
26. Izumi, F.; Momma, K. Three-Dimensional Visualization in Powder Diffraction. *Solid State Phenom.* **2007**, *130*, 15–20. [[CrossRef](#)]
27. Matsumoto, R.; Sasama, Y.; Fujioka, M.; Irifune, T.; Tanaka, M.; Yamaguchi, T.; Takeya, H.; Takano, Y. Note: Novel diamond anvil cell for electrical measurements using boron-doped metallic diamond electrodes. *Rev. Sci. Instrum.* **2016**, *87*, 076103. [[CrossRef](#)] [[PubMed](#)]
28. Matsumoto, R.; Irifune, T.; Tanaka, M.; Takeya, H.; Takano, Y. Diamond anvil cell using metallic diamond electrodes. *Jpn. J. Appl. Phys.* **2017**, *56*, 05FC01. [[CrossRef](#)]
29. Matsumoto, R.; Yamashita, A.; Hara, H.; Irifune, T.; Adachi, S.; Takeya, H.; Takano, Y. Diamond anvil cells using boron-doped diamond electrodes covered with undoped diamond insulating layer. *Appl. Phys. Express* **2018**, *11*, 053101. [[CrossRef](#)]
30. Mao, H.K.; Bell, P.M.; Shaner, J.W.; Steinberg, D.J. Specific volume measurements of Cu, Mo, Pd, and Ag and calibration of the ruby R₁ fluorescence pressure gauge from 0.06 to 1 Mbar. *J. Appl. Phys.* **1978**, *49*, 3276–3283. [[CrossRef](#)]
31. Akahama, Y.; Kawamura, H. High-pressure Raman spectroscopy of diamond anvils to 250 GPa: Method for pressure determination in the multimegabar pressure range. *J. Appl. Phys.* **2004**, *96*, 3748–3751. [[CrossRef](#)]
32. Higashinaka, R.; Miyazaki, R.; Mizuguchi, Y.; Miura, O.; Aoki, Y. Low-Temperature Enhancement in the Upper Critical Field of Underdoped LaO_{1-x}F_xBiS₂ (x = 0.1–0.3). *J. Phys. Soc. Jpn.* **2014**, *83*, 075004. [[CrossRef](#)]
33. Matsumoto, R.; Hou, Z.; Hara, H.; Adachi, S.; Tanaka, H.; Yamamoto, S.; Saito, Y.; Takeya, H.; Irifune, T.; Terakura, K.; et al. Crystal Growth, Structural Analysis, and Pressure-Induced Superconductivity in a AgIn₅Se₈ Single Crystal Explored by a Data-Driven Approach. *Inorg. Chem.* **2019**, *59*, 325–331. [[CrossRef](#)] [[PubMed](#)]
34. Wu, S.F.; Richard, P.; Wang, X.B.; Lian, C.S.; Nie, S.; Wang, J.T.; Wang, N.L.; Ding, H. Raman scattering investigation of the electron-phonon coupling in superconducting Nd(O,F)BiS₂. *Phys. Rev. B* **2014**, *90*, 054519. [[CrossRef](#)]
35. Tian, Y.; Zhang, A.; Liu, K.; Ji, J.; Liu, J.; Zhu, X.; Wen, H.-H.; Jin, F.; Ma, X.; He, R.; et al. Raman scattering in superconducting NdO_{1-x}F_xBiS₂ crystals. *Supercond. Sci. Technol.* **2015**, *29*, 15007. [[CrossRef](#)]
36. Lorenz, B.; Meng, R.L.; Chu, C.W. High-pressure study on MgB₂. *Phys. Rev. B* **2001**, *64*, 012507. [[CrossRef](#)]
37. McMillan, W.L. Transition Temperature of Strong-Coupled Superconductors. *Phys. Rev.* **1968**, *167*, 331–344. [[CrossRef](#)]